pH and ion-selective swelling behaviour of keratin and keratose 3D hydrogels

Gonzalo Galaburri, María L. Peralta Ramos, Juan M. Lázaro-Martínez, Roberto Fernández de Luis, María Isabel Arriortua, María E. Villanueva, Guillermo J. Copello

PII: S0014-3057(19)30362-3
DOI: https://doi.org/10.1016/j.eurpolymj.2019.05.043
Reference: EPJ 9064

To appear in: *European Polymer Journal*

Received Date: 22 February 2019
Revised Date: 16 May 2019
Accepted Date: 20 May 2019

Please cite this article as: Galaburri, G., Peralta Ramos, M.L., Lázaro-Martínez, J.M., Fernández de Luis, R., Isabel Arriortua, M., Villanueva, M.E., Copello, G.J., pH and ion-selective swelling behaviour of keratin and keratose 3D hydrogels, *European Polymer Journal* (2019), doi: https://doi.org/10.1016/j.eurpolymj.2019.05.043

pH and ion-selective swelling behaviour of keratin and keratose 3D hydrogels

Gonzalo Galaburri[a], María L. Peralta Ramos[a], Juan M. Lázaro-Martínez[b,c], Roberto Fernández de Luis[d], María Isabel Arriortua[e], María E. Villanueva[a,b], Guillermo J. Copello[a,b,*]

[a]*Universidad de Buenos Aires (UBA), Facultad de Farmacia y Bioquímica, Departamento de Química Analítica y Fisicoquímica, (UBA), Junín 956, C1113AAD, Buenos Aires, Argentina;*

[b]*CONICET - Universidad de Buenos Aires. Instituto de Quı́mica y Metabolismo del Fármaco (IQUIMEFA), Junı́n 956, C1113AAD, Buenos Aires, Argentina;*

[c]*Universidad de Buenos Aires (UBA), Facultad de Farmacia y Bioquímica, Departamento de Química Orgánica, Junín 956, C1113AAD Buenos Aires, Argentina;*

[d]*BCMaterials (Basque Centre for Materials, Applications & Nanostructures), Bld. Martina Casiano, 3rd. Floor UPV/EHU Science Park Barrio Sarriena s/n 48940 Leioa, Spain.*

[e]*Universidad del País Vasco (UPV/EHU), Departamento de Mineralogía y Petrología, Barrio Sarriena s/n, 48940, Leioa, Spain.*

*Corresponding Author.

E-mail address: gcopello@ffyb.uba.ar (G.J. Copello)

ABSTRACT

The oxidation of keratin hydrogels was optimized aiming to obtain keratose hydrogels while maintaining the original 3D structure and pH-responsive behaviour. In addition, we present a comparative study of their dual-stimuli responsive behaviour regarding the pH-responsiveness and their previously non-described ion selective responsiveness. Keratose and keratin hydrogels showed similar swellings when contracted at low pH, and the former showed steeper expansion and higher swelling than the latter at high pH. In addition, both hydrogels showed selective responsiveness toward Ca^{2+} ions when expanded, and toward Cu^{2+} ions when contracted. IR, Raman, *ss*-NMR, HRMAS NMR, SAXS, and thermal characterization demonstrated that oxidation does not interfere with the stimuli-responsive mechanisms related to protein conformation. The higher swelling of keratose hydrogels would be originated in the increase of the mobility of the chains after oxidation coupled to the hydration of sulfonic acid groups.

Keywords: keratin, hydrogel, keratose, smart material, stimuli-responsive

1. Introduction

Keratins are a group of cysteine-rich filament-forming proteins, as well as the second most essential and abundant biopolymer found in animals. It is present in the epidermal appendages of cattle and poultry, like nails, claws, beak, hair, wool, horns, and feathers [1]. Thus, it is one of the main waste products generated by the livestock industry. In the search for the replacement of oil-based polymers, this renewable and disposable natural polymer is one of the most promising candidates for the development of innovative biomaterials. Not only its low cost and renewability, but also its biodegradability and biocompatibility are features to take into account [2,3]. Nevertheless, fundamentals of the chemistry and structure of keratin protein are still not completely understood, being this information one of the keys that could pave the way to the processing of keratin as versatile products.

Keratin is a tightly packed structural protein with a high number of disulfide bridges, hydrophobic interactions, and hydrogen bonds. The peculiar structure of keratin confers indissolubility, mechanical stability, and resistance to common proteolytic enzymes and chemicals. Thus, it is imperative to extract and dissolve keratins from animal keratinous materials. Most of the current processes for its extraction are based on reductions, oxidations, strong acid or alkali hydrolysis and other violent reaction paths, which are not

environmentally friendly and/or result in severe degradation and destruction of keratins [4,5]. Among keratin-based products, if oxidative conditions are used, the obtaining methodology may lead to a different protein: keratose. Keratose is generated by the oxidation of thiol or disulfide linkages to sulfonic acid groups [6]. It presents distinctive behaviour respect from keratin materials while maintaining many of their advantageous properties [6,7]. As it could be expected, keratin materials processing is a key feature to take into account. In order to seize the desirable properties of keratin, and overcome its drawbacks, several studies have reported the chemical modification of the protein. In this regard, keratin -SH have converted to allyl thioether in order to obtain a photopolymerizable gel and grafted with photosensitizers for the obtaining of antibacterial sponges [8,9].

From another perspective, in views of the promising and versatile applications of smart materials, many of these chemical modifications aim to endow the material with stimuli-responsive behaviour. For example, Ham et al. have alkylated human hair keratin for the control of erosion and drug delivery, and Guo et al. have used methacrylic acid, N-isopropyl acrylamide and itaconic acid for grafting keratin hydrogels in order to endow them with pH and thermo-responsiveness [2,10,11]. From a different approach, without the use of chemical modifications or grafting polymers, the Peralta Ramos partial hydrolysis method lead to a smart keratin hydrogel that can be obtained by using environmentally friendly reagents [12]. The smart hydrogels developed by this method have demonstrated interesting potentialities in the field of water treatment and infection prevention [13,14]. Despite the broad scope of approaches used to obtain Keratose from Keratin, the stimuli-response behaviour of this bio-polymer still remains to be fully understood and needs further study. The relevance of the study of these materials relays in their applicability in many fields. Among other applications, responsive hydrogels have been used in designing micromanipulators, microfluidic valves, sensors, and optical devices with tunable focal length [15]. In particular, natural polymers, such as keratin, are promising materials as tissue engineering scaffolds, selective cell adhesion matrices and drug delivery systems in the biomedical field, due to their hydrophilic nature and biocompatibility [16].

In this work, we present the optimization of keratin smart hydrogels oxidation for the obtaining of keratose hydrogels which maintain the original 3D structure and pH-responsive behaviour. In addition, we present a comparative study of their dual-stimuli responsive behaviour regarding the aforementioned pH-responsiveness and, to the best of our knowledge, a non-described selective ion-responsiveness behaviour in these materials. The optimization of the oxidation and the mechanism of the stimuli-responsive behaviour were

analysed by ATR-IR, Raman spectroscopy, *ss*-NMR, HRMAS NMR, thermal analysis, SAXS, and SEM.

2. Experimental section

2.1. Materials

Sodium hydroxide, K_2HPO_4, KH_2PO_4 were purchased from Anedra (Argentina). Ethanol 96% was acquired from Soria (Avellaneda, Argentina). Ethyl Acetate was purchased from Sintorgan (Argentina). Hydrogen peroxide 30% from Stanton (Argentina). All other reagents were of analytical grade. Whole cow's horns (*Bos taurus*, Hereford) were kindly donated by Frigorina (La Plata, Buenos Aires, Argentina) and used as keratin source.

2.2. Preparation of keratin (Ker) hydrogels

Horns were milled and sieved through a 250 μm sieve. Then, the horn powder was washed three times with distilled water and three times with ethyl acetate to remove fat. After that, the powder was dried at 37 °C overnight. Keratin (1 g) powder was mixed with 7 ml dilution of NaOH 1 M in Ethanol (25 ml). The mixture was left at 45 °C for 4 h. Afterwards, the mixture was homogenized through a syringe and left until complete dryness at 45 °C. This material was thoroughly washed with distilled water in order to remove all NaOH residue. After hydration, the hydrogel form of the material was obtained.

2.3. Preparation of keratose (Kox) hydrogels

Keratose hydrogels (Kox) were obtained by H_2O_2 oxidation of the keratin hydrogels. Approximately 0.4 g of dry hydrogel were immersed in 50 ml of the oxidant solution in open flasks. Different oxidant conditions were assayed. Hydrogen peroxide concentration was assayed between 5 and 30%, and temperatures ranged from 4 to 60 °C, with 16 h incubation times. The obtained keratose was washed with several volumes of distilled water.

For each oxidation condition, a whole Ker hydrogel was divided into two pieces. One piece was oxidized at a certain condition and the other piece was kept as a control for comparison. The oxidation from keratin to keratose was followed by comparing the area of the 1040 cm^{-1} band corresponding to S=O stretching vibration by FT-IR spectroscopy.

2.4. Spectroscopic characterization

ATR-FTIR (diamond attenuated total reflectance) and FT-Raman were recorded using a Nicolet iS50 Advanced Spectrometer (Thermo Scientific). ATR-FTIR spectra were

acquired with 32 scans and a resolution of 4 cm^{-1}. The oxidation was evaluated by determining the area of the 1040 cm^{-1} band, corresponding to the S=O groups. For each spectrum, the 1040 cm^{-1} peak area was measured after setting a baseline between 1020 and 1060 cm^{-1}. Then, the area of Amide I band, at 1635 cm^{-1} was measured after setting a baseline between 1600 and 1670 cm^{-1}. Amide I band area was used as the reference peak and the A_{1040}/A_{1635} ratio was calculated and compared among treatments.

FT-Raman spectra were acquired with an excitation laser beam of 1064 nm, 0.5 W laser power, resolution of 8 cm^{-1}, 100 scans. All samples were previously dried for 24 h at 60 ºC to avoid water-related bands interference. Amide I band (1690-1640 cm^{-1}) was deconvoluted for the analysis of the α-helix (1655 cm^{-1}) and β-sheets (1679 cm^{-1}) components. Spectral baselines were set between 1750 and 1503 cm^{-1}, taking in consideration the overlapping of the ν(C═C) olefinic band (1604 cm^{-1}) with the amide I band. Spectra decomposition was performed using Fityk software [17] assuming a Lorentzian shape for narrow peaks (α-helix and olefinic band) and a Gaussian form for broad peaks (β-sheets) [18].

X-ray photoelectron spectra were acquired using a Specs (Berlin, Germany) system equipped with a Phoibos 150 1D-DLD analyser, monochromatic AlKα radiation (1486.6 eV, 300 W, 13 kV) and a multi-channel detector. Spectra were recorded in the constant pass energy mode at 100 eV for survey spectra. The binding energy of the adventitious carbon (C1s) was set at 284.6 eV to correct sample charging. The spectra were fitted with the CasaXPS 2.3.19 software, which models the Gauss–Lorentzian contributions.

The investigation of the nanostructure of the dried materials and the hydrogels swelled and equilibrated in the range of pH 4 to 8 or equilibrated in a 100 mM $CaCl_2$ solution was performed by Small Angle X-ray Scattering (SAXS) using the SAXS1 beamline of the National Synchrotron Light Laboratory (LNLS), Campinas, Brazil. The SAXS measurements were performed at room temperature in transmission geometry with λ=1.55 Å (8 keV). The 2D SAXS spectra were monitored using a Pilatus 300K detector. A sample-to-detector distance of 1.5 m and 6 exposures of 10 s and were used for each sample. The samples were placed with their surfaces perpendicular to the direction of the incident X-ray beam and parallel to the X-ray detector. The scattering intensity (I) was measured as a function of the scattering vector (q) from 0.06 to 2.9 nm^{-1}. The background and parasitic scattering were determined by using an empty sample holder and were subtracted for each measurement. SAXS 2 D images and scattering profiles were analysed with Bioxtas Raw software and data modelling was performed using SASfit software [19,20].

The solid-state Nuclear Magnetic Resonance (*ss*-NMR) experiments were acquired using a Bruker Avance-III HD spectrometer, equipped with a 14.1 T narrow-bore magnet operating at Larmor frequencies of 600.09 MHz for ^{1}H and 150.91 MHz for ^{13}C. Powdered samples were packed into 3.2-mm ZrO_2 rotors and rotated at magic angle spinning (MAS) at room temperature. Glycine was used as an external reference for the ^{13}C spectra and to set the Hartmann−Hahn matching condition in the cross-polarization and magic angle spinning (CP-MAS) experiments in ^{13}C spectra at a MAS rate of 15 kHz. The contact time during CP was 2000 μs. The SPINAL64 sequence (small phase incremental alternation with 64 steps) was used for heteronuclear decoupling during acquisition. The number of scans was 4000. The different hydrogels were analysed by ^{1}H high-resolution magic angle spinning (HRMAS) NMR experiments by packing the swelled samples with D_2O into a 4-mm ZrO_2 HRMAS rotor with a 50 μL spherical insert and the sample was spun at 4 kHz. A presaturation pulse sequence was applied for the suppression of the water proton signals.

2.5. Microscopic Characterization

Electron microscopy images were obtained on a Zeiss Supra 40 scanning electron microscope (SEM). The hydrogels swelled at different conditions were freeze-dried and coated with gold, before the observation.

2.6. Thermal analysis

Thermogravimetric (TG) and Differential Scanning Calorimetry (DSC) analysis were carried out using a NETZSCH STA 449F3 thermo-balance. An alumina crucible containing approximately 0.015 g of a dried sample was heated at 5 °C/min in the temperature range 25-700 °C under synthetic air and nitrogen atmosphere.

2.7. Swelling studies

In order to assess the swelling behaviour of the material in different conditions, 0.02 g of a dried Ker and Kox were equilibrated in different 10 mM phosphate solutions ranging from pH 3 to pH 8 and diverse electrolyte solutions containing NaCl, $CaCl_2$, $MgCl_2$, and $CuCl_2$ ranging from 0 to 500 mM. Before hydration and after equilibrium was reached, the hydrogels were removed from the solution and accurately weighted. The swelling percentage was calculated as follows:

Sw% = (Swelled weight – Dry weight)*100/Dry weight

2.8. Point of Zero Charge determination

The point of zero charge (pH_{pzc}) of the dry keratin material was determined by the drift method [21]. Briefly, a solution of 0.01 M NaCl, was boiled to remove dissolved carbon dioxide and used to prepare several solutions with an initial pH ranging from 4 to 8. Then, 0.05 g of Ker or Kox were added to 10 ml of each solution and incubated at room temperature for 48 h. The final pH was measured and plotted against the initial pH. The pH point at which the curve of the final pH crosses the $pH_{initial}$=pH_{final} line is the pH_{pzc}.

2.9. Statistics

All experiments and their corresponding measurements were conducted in triplicate under identical conditions and statistically analysed by one-way ANOVA and by Bonferroni Multiple comparison post-test if ANOVA $p<0.05$. Data were expressed as mean ± standard deviation (SD). A value of $p<0.05$ was considered to be statistically significant. R language and environment was used for statistical computing and graphics [22].

3. Results and discussion

3.1. Effect of oxidation conditions

The Ker hydrogels are stiff 3D structures and easy to manipulate without altering their shape. In a previous work, it was stated that the hydrogel form of keratin is achieved by partial hydrolysis, which implies the reduction of -S-S- bridges into -SH, allowing the protein chains to acquire higher mobility and higher hydration states [12]. The optimization of the oxidation aimed the maximum oxidation of keratin -SH groups without altering other moieties, while maintaining the 3D structure of the hydrogel. The effect of oxidation conditions was evaluated regarding H_2O_2 concentration, temperature and time. The incubation time was fixed at 16 h to ensure completeness of the reaction. Shorter incubation times led to non-reproducible oxidation. Temperatures higher than 25 °C altered the 3D structure of the hydrogel, as can be seen in Figure SD1 of the Electronic Supplementary Data (SD).

3.2. Infrared, Raman, solid state NMR and XPS spectroscopic characterization

Infrared, Raman, NMR and XPS spectroscopies were chosen to characterize the changes suffered by the keratin hydrogels after the oxidation process. Both the Raman and ss-NMR, as well as the Infrared spectra showed little variations in the chemical structure of the keratin and keratose materials (Figure 1 and 2). This was expected since maintaining the

hydrogel main properties was desired. The FT-Raman spectra (Figure 1a) confirmed the stability of the carbon structure after oxidation but with a slight change in the relation of intensities of the 1665 cm^{-1} band (amide I) and 1604 cm^{-1} (olefinic groups). The symmetry of the Amide I band depended on the general conformation of the chains of the proteins. This is an unresolved C-N peak of amide in α-helix, β-sheet, and less ordered states [23]. The deconvolution of Amide I peak demonstrated that the areas of α-helix and β-sheets components of this band varied after the oxidation (SD 2). The β-sheets-to-α-helix peak area ratio varied from 1.55 to 0.66, indicating a relative decrease of the β-sheets component. This would indicate that the conformation of keratin changed in its passage to keratose.

The analysis by solid state ^{13}C CP-MAS NMR (Figure 1b) of the dry Ker and Kox, confirmed that the main carbon structure of keratin was maintained after the oxidation treatment. The ^{13}C CP-MAS spectra of both Ker and Kox materials showed typical carbon skeletal protein signals corresponding to the sp^3 region ($\delta^{13}C$ = 80-0 ppm), such as the aliphatic carbons of the side chains between 10-40 ppm, the alpha carbon resonance signals (-NH-**C**HR-CO-) at 50-70 ppm, as well the specific signals associated with the residues of *Ser* (OH-**C**H_2-) and *Thr* (CH_3-**C**H(OH)-) residues. Also, the sp^2 region ($\delta^{13}C$ = 200-100 ppm) shows the carbonyl resonance signal of the peptide bonds at 180-170 ppm well as some carbons associated with *Tyr* and *Phe* residues at 158 and 130 ppm, respectively. When comparing Ker and Kox spectra, it can not be observed the appearance of new peaks or the disappearance of pre-existing ones. Moreover, no significant peak shift or relative intensity variation could be detected.

Figure 2 showed the FT-IR spectra of Ker and Kox obtained using different amounts of H_2O_2. After a thorough comparison between the infrared spectra, it could be seen that no appreciable changes in the keratin chemical structure arise in this stage. Thus, the FT-IR, Raman and ^{13}C CP-MAS NMR spectra showed that most of the primary sequence of the polypeptide remained intact. Nevertheless, a small sharp band at 1040 cm^{-1}, accounting for S=O groups, was only detected in the Kox hydrogels' spectra, proving that the oxidation process was successful (SD 3) [7]. Also, since there is no modification of the pre-existent bands from Ker spectrum it could be presumed that the oxidation was mainly selective for the oxidation of -SH groups of cysteine in -S=O groups of cysteic acid. The relative intensity of this band increased along with H_2O_2 concentration. This was supported by the analysis of the XPS spectra of the materials at the S 2p zone shown in Figure 2c and d. The spectra indicated that after the oxidation the proportion of the -SO_3^- groups (168.8 eV) increased significantly

and confirmed the oxidation of the -SH groups (164.0 eV) [24]. It is also worthy to indicate that ker materials also presented these groups, pointing that the main mechanism of the -S-S- cleavage would be the hydrolysis originally proposed by Florence [25]. In this reaction some of the -S-S- moieties are converted into sulfinic acid.

The oxidation from keratin to keratose was evaluated by FT-IR spectroscopy by determining the area of the 1040 cm^{-1} band, corresponding to S=O stretching vibration, using Amide I band, at 1635 cm^{-1}, as reference band. The effect of H_2O_2 concentration and temperature on the oxidation can be observed in Figure SD 4. The incubation of Ker at 25 °C in a 20 % H_2O_2 solution showed the highest -S=O obtaining. Although there are no significant differences between the incubation at 20 % and 30 % H_2O_2 solutions, the latter showed a higher standard deviation, which is probably due to an undesirable extension of the oxidation. Thus, incubations at 20 % H_2O_2 were chosen for the following due to its higher reproducibility. The temperature showed to be less influential in -S=O generation. No significant differences were observed among different temperature treatments. Nevertheless, as mentioned before, a loss of the 3D structure was observed when incubations above 25 °C where used. Therefore, incubations at 20 % H_2O_2 and 25 °C were chosen as the optimum conditions for Kox hydrogel obtaining.

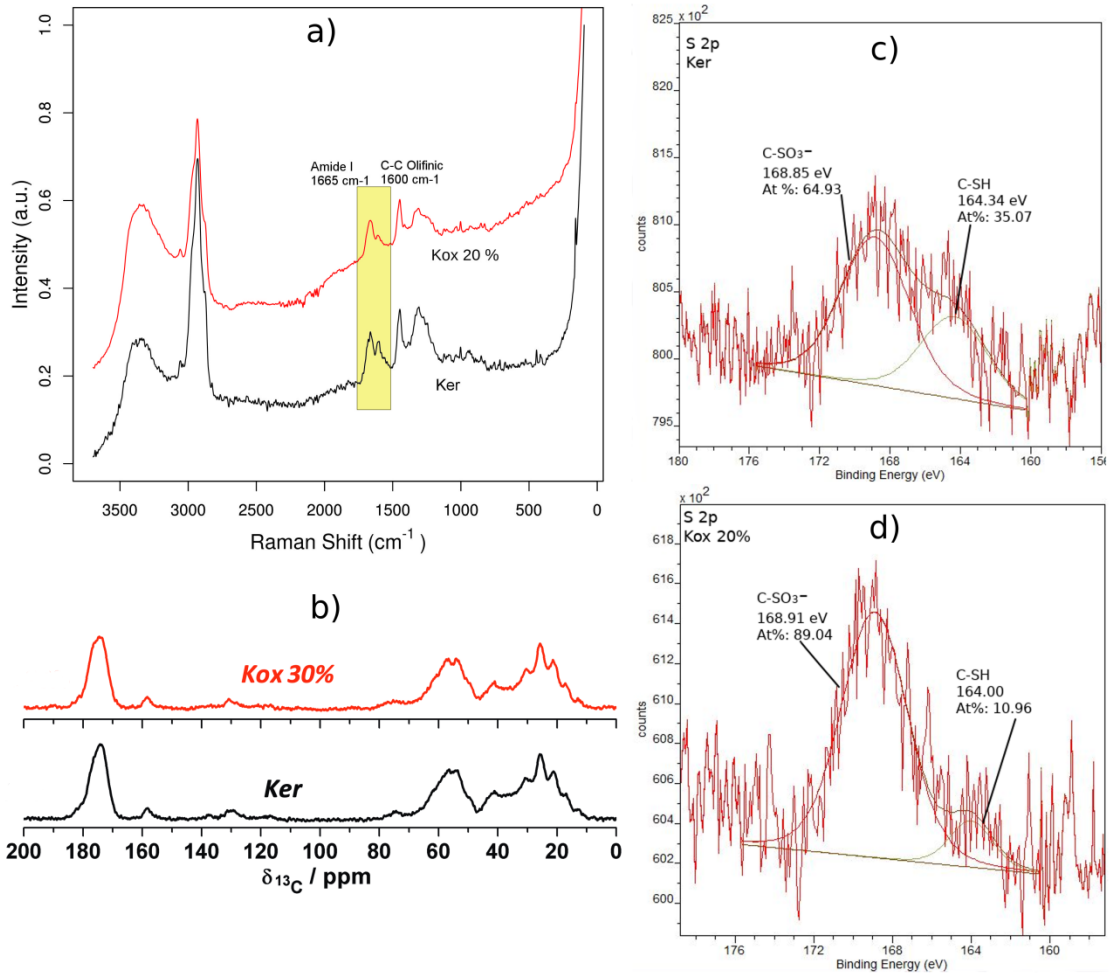

Figure 1. a) FT-Raman, b) ^{13}C CP-MAS NMR (@ 15kHz), c) and d) XPS spectra of Ker and Kox dry materials.

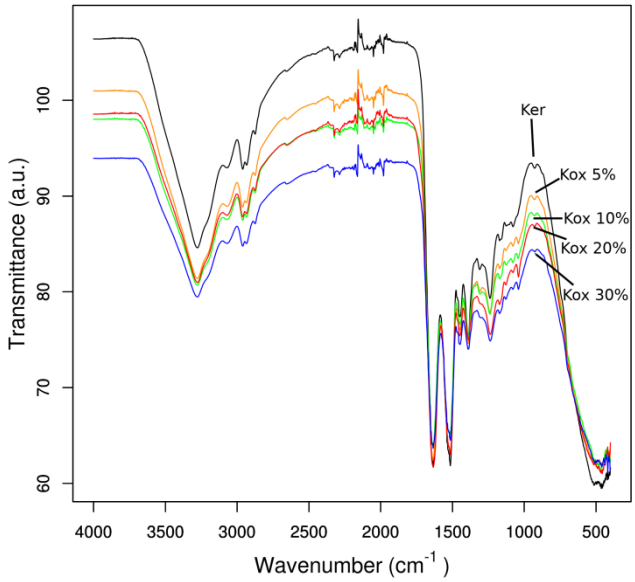

Figure 2. ATR-IR spectra in the range of 4000-400 cm^{-1} of Ker and Kox obtained using different amounts of H_2O_2.

3.3. Thermal analysis

The thermal behaviour of the Ker and Kox hydrogels was assessed by DSC and TG under N_2 and Air atmospheres, as can be seen in Figures 3 and SD 5-7. Under N_2 protective atmosphere, the DSC profiles of both Ker and Kox showed a toughening transition between100 and 200 °C in contrast to the typical glass transition expected in many polymers.[26] In this transition, tightly bound water would be removed allowing new interchain interactions to occur, leading to a toughening rather than a softening. At 236 °C for Ker and 221 °C for Kox the melting temperature (*Tm*) can be observed as an endothermic event. This peak has been ascribed to the denaturation of keratin crystalline structure, being lower temperatures reported for less crystalline keratins [27]. These would imply a change in the Ker nanostructure when it was oxidized to Kox. For both Ker and Kox, at 278 °C is evident the endothermic peak corresponding to the decomposition of the polypeptide chain [27,28]. In Kox's thermal profile this peak is clearly broader than for Ker. This is probably due to the mobility of the chemical groups in the tight network rather than the difference in chemical composition. In support of this assumption, the TG profiles under N_2 atmosphere of Ker and Kox are almost identical, indicating that the chemical oxidation did not alter the thermal stability of the protein under a protective atmosphere. Thus, the differences observed in the DSC profile would rather account for changes in the polypeptide conformation than for the chemical oxidation. The main differences in the TG of the samples was a higher mass loss for Kox at temperatures starting around 50 °C, which probably accounted for the evaporation of water in the higher hydrated surface of this sample (12%) respect the Ker one (8%). In both profiles, the mass loss is incomplete reaching 26 % of the initial mass. This has also been reported for other types of keratins in nitrogen atmosphere [29]. On the other hand, for the TG under air atmosphere (SD 6), the mass loss is complete for Kox, which implies that oxidative processes were needed for the complete mineralization, while for Ker, the mineralization is not complete even in air atmosphere (7% residual mass). SD 7 shows the DSC thermogram under air atmosphere. In these thermograms, it could be seen at 507 °C and 586 to 595 °C exothermic peaks for Ker and Kox, that were absent under protective atmosphere (SD 5). Also, although it had been reported that the decomposition of Sulfur-containing moieties started above 250 °C, this peaks probably accounted for thermal stable adducts formed during decomposition [28].

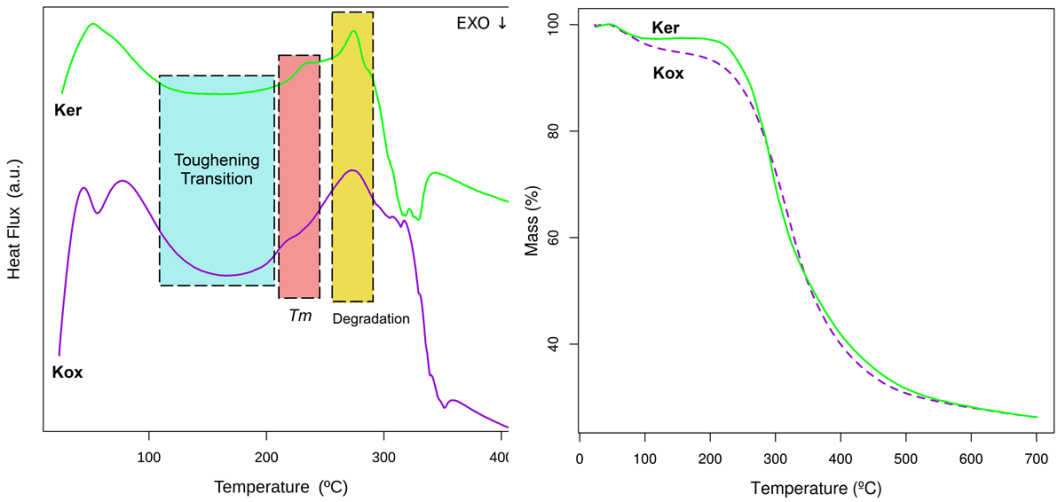

Figure 3. DSC a) and TG b) thermograms under N_2 atmosphere of the Ker and Kox 20% dry materials.

3.4. Swelling studies and point of zero charge determination

The swelling behaviour of the materials was assessed by means of its water uptake against pH and the ion composition of the surrounding media. Both Ker and Kox hydrogels showed reversible pH and ion responsive behaviour Figure 4 shows the swelling behaviour at different media pHs. The swelling inflection point at which the hydrogels went through the contracted to the expanded state appeared in both cases between pH 5 and 6. From these results, it could be inferred that the introduction of new $-SO_3^-$ groups do not alter the swelling behaviour regarding the inflection point. In a previous work, it had been pointed out that the keratin hydrogels' pH-responsiveness did not correspond to electrostatic repulsion but to a conformational change in the protein, which associated with the protonation state of their -COOH groups and the interchain interactions [12]. The fact that the introduction of $-SO_3^-$ in the material did not alter the inflection point reinforces this assumption. In fact, as can be seen in Figure 4, the pH_{pzc} of Ker is 6.8 and Kox 5.5, showing that the net charge at the different pH values differs from one sample to the other. This implies that although the introduced acidic groups were capable of diminishing the pH_{pzc}, the protein conformation at each pH is responsible for its swelling rather than the repulsion between these groups.

At lower pH values the behaviour of Ker and Kox regarding swelling % was similar

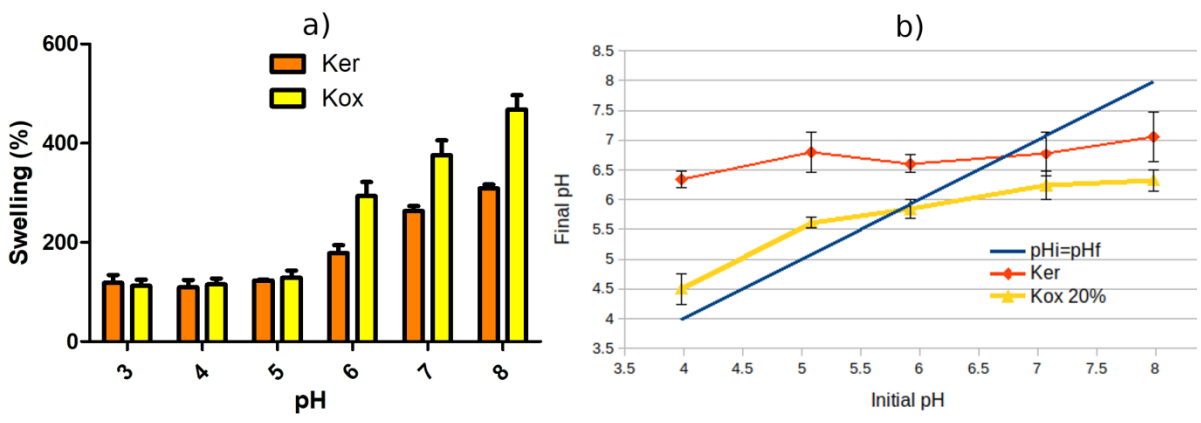

(p>0.05, pH: 3, 4, 5). However, beyond the inflection point, Kox showed higher swelling % than Ker (p<0.01, pH: 6, 7, 8). This difference led to a steeper variation between the contracted and the expanded state in Kox (p<0.001 for Kox and p<0.05 for Ker). These differences are due to the higher swelling of Kox respect to Ker. Probably, the introduction of negatively charged -SO_3^- groups may have affected the protein conformation in two ways that would lead to the higher swelling. First, the repulsion between the charged groups would interfere with a tight folding, allowing higher amounts of water to enter among the polypeptide chains. Second, the presence of -SO_3^- groups in the chain surface would imply a higher solvation state than for -SH groups. This will be discussed below, together with HRMAS NMR results.

Figure 4. a) Swelling behaviour and b) Point of Zero Charge of Ker and Kox 20% hydrogels.

The responsive behaviour was also evaluated against different concentrations of monovalent and divalent electrolytes: NaCl, $CaCl_2$, $MgCl_2$ and, $CuCl_2$. As could be seen in Figure 5, at pH 8, where the Ker and Kox were expanded, only high molarities of Na^+ and Mg^{2+} lead to significant contractions of both types of gels. However, the influence of Ca^{2+} was significant in terms of the steep decay in swelling that was induced when Ca^{2+} molarity increases from 10 to 50 mM (p<0.001). At pH 3, where the samples were in the contracted state, there was no significant influence of Na^+ or Ca^{2+} in the swelling, whereas Cu^{2+} significantly increased the swelling of both Ker and Kox when 10 mM of the ion is added to the solution (p<0.001). Above 10 mM Cu^{2+}, the swelling decreases. Probably, at higher Cu^{2+} concentrations, the ionic force effects overrule the swelling increase and the contraction of the gel is the resulting consequence.

It has been previously reported that salt concentration may influence keratin assembly, and monovalent ions concentration, such as K^+, can influence keratin mechanical properties [30,31]. Nevertheless, the ion responsive behaviour of both Ker and Kox seems not to be related to the valence of the cations. Again, this can be associated with the conformation of the polypeptide chains rather than the repulsion among the chains and the effect of charge neutralization given by the ions. Thus, the ion-responsiveness at the contracted and the expanded states appears selective to specific ions. Probably, this arises in relation to their interaction to moieties of the polypeptide chain that are involved in interchain interactions driving the folding of the secondary structure of the protein. The existence of a 3D hydrogel network is possible due to tight protein-protein interactions and the swelling is driven by the presence of mobile chains capable to adsorb higher amounts of water. Probably, the more

mobile chains are the responsible for the selective interactions with the ions, with the consequent swelling variations, and their specific folding is in turn restricted by protein-protein interactions. Several possible applications mainly in the field of sensors and actuators may arise from the observation of the differences in the steepness of the swelling variation against pH and specific ions. Nevertheless, due to the difference in the pH_{pzc}, it is possible that for some applications the use of Ker hydrogels would be more desirable than Kox. In order to understand the reasons that lead to the higher swelling of Kox respect Ker at the expanded state and the ion selective responsive behaviour, electron microscopy, ^{1}H HRMAS NMR and SAXS determination were performed.

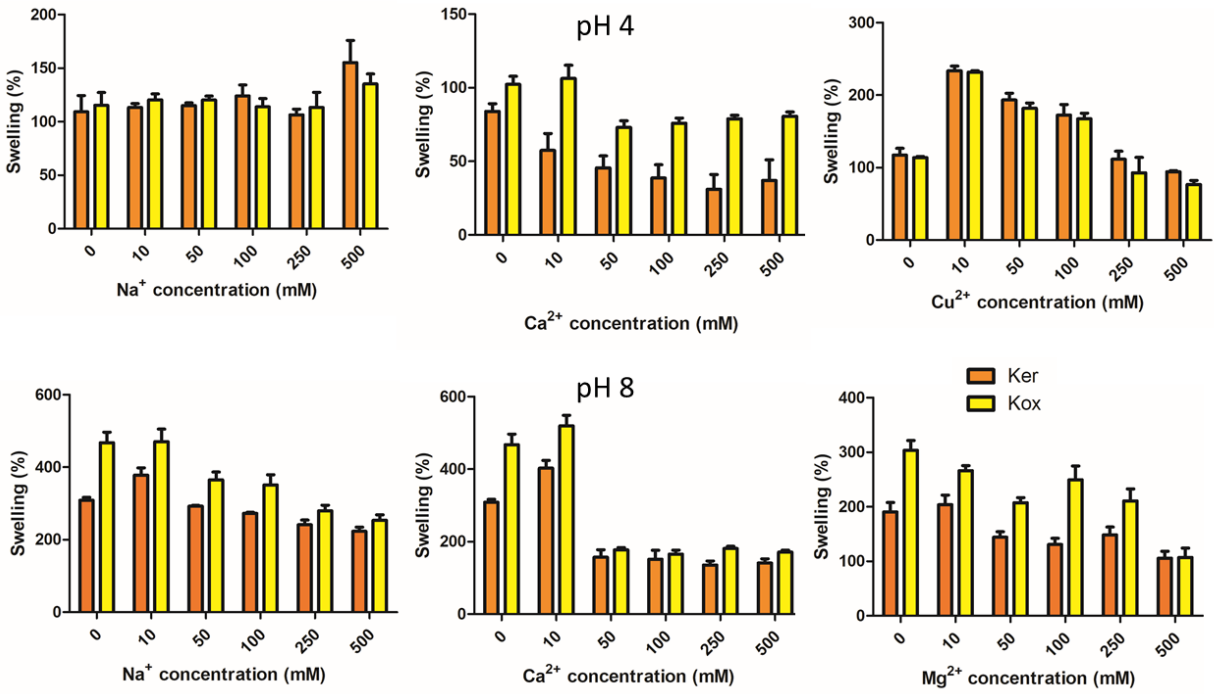

Figure 5. Swelling behaviour of the hydrogels vs cation ions.

3.5. Microscopic characterization

Microscopic images agreed with the swelling assays. This was evidenced in SD 9 where the images of freeze-dried Ker and Kox hydrogels presented collapsed structures at low pHs and expanded structures with high porosity at higher pHs. In addition, when the hydrogels were exposed to a 100 mM Ca^{2+} solution the topography observed was the one of a contracted structure (SD 10), as expected from the swelling assays.

3.6. ^{1}H HRMAS NMR of swelled hydrogels

Further insight into the effect of the H_2O_2 concentration and temperature was acquired through studying the hydrated materials by ^{1}H HRMAS NMR, as it is presented in Figure 6

and SD 11. In agreement with the solid-state ^{13}C CP-MAS NMR, at the swelled state there were no clear changes from the appearance or disappearance of peaks after the oxidation. The most significant variations appeared at 8.3 ppm and 1.9 ppm peaks where it could be seen the increase of the relative intensity of these signals together with the increase of H_2O_2 concentration and the increase in the incubation temperature. These signals would account for amide protons and amino acids aliphatic side chains protons respectively [32,33]. Since the oxidative treatment was not related to the addition of new amide bonds or aliphatic residues, the increase in these signals would be associated with the gain in local mobility of these moieties. Since HRMAS NMR measurement was performed at the swelled state, the behaviour of the sample was neither the one of a liquid nor the one of a solid. When NMR measurements are performed in the solid state, the dipolar interaction is strong enough to broaden the signal when compared to solution-state NMR, where the dipolar coupling is averaged by Brownian motion leading to sharp signals. For polymeric substances, as higher the chain mobility, more liquid-like will be the NMR signal. Thus, the addition of $-SO_3^-$ groups would probably be introducing higher interchain repulsion and/or the higher hydrophilicity of these groups would lead to the distancing of the polypeptide chains due to their higher solvation state. The diminishing in amide proton intensity that could be observed when 30 % H_2O_2 concentration or temperatures higher than 25 °C were used during oxidation could be related to certain degradation of the polypeptide structure. Moreover, there are some other changes present in the swelled state corresponding to amide and or aromatic protons at a ^1H chemical shift around 7.25-7.75 ppm in Kox 10% (Figure 6) and also in Kox 20% at 45ºC (Figure SD 11). In this sense, the ^1H HRMAS spectra revealed more detailed information at the atomic scale in the swelled state than the information obtained from the ^{13}C CP-MAS spectra (Figure 2b). In the ^{13}C CP-MAS *ss*-NMR experiments the signals are coming mainly from ordered regions of the peptide structure where the dipolar interactions are stronger than in disorder regions explaining that the ^{13}C CP-MAS spectra of the Ker and Kox samples did not present changes [34].

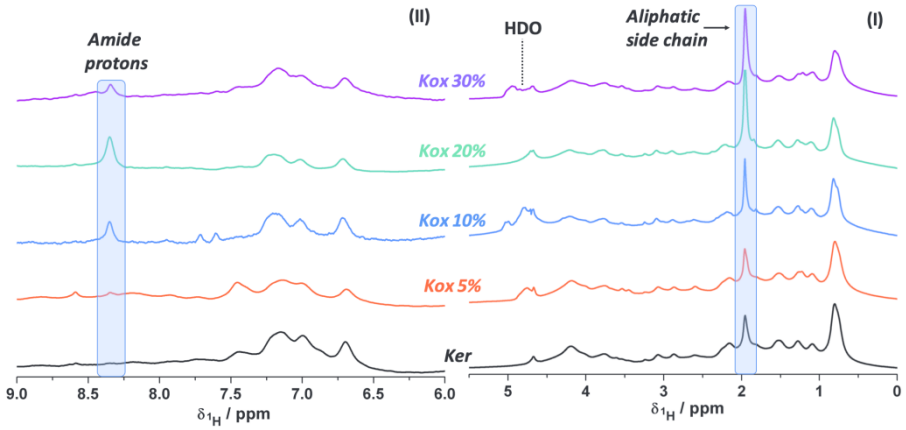

Figure 6. ^{1}H HRMAS NMR (@ 4kHz) spectra for Ker and Kox hydrogels swelled in D_2O obtained using different amounts of H_2O_2.

3.7. Small Angle X-ray Scattering (SAXS)

The variations in the nanometric structure of Ker and Kox hydrogels and the dry materials regarding the influence of pH and ion responsiveness was assessed by SAXS. Figure 7 shows the SAXS profiles from the dry material and the hydrated material. By comparison among the trends of Ker and Kox SAXS profiles, it could be concluded that the oxidation did not affect significantly the overall nanometric structuration of the polypeptide chains. This fact was evidenced when comparing the profiles of the Ker and Kox samples with similar treatments. All samples showed a power-law profile at low q. These profiles were characteristic of materials without a specific or unique shape, such as disordered and semicrystalline polymers. The α slope of the $I(q)\sim q^{-\alpha}$ relation at the power-law section was indicative of the conformation that the polymeric chains adopted in the material. For both dry materials, the power-law behaviour persists up to 0.038 Å^{-1}. The dry materials presented slopes between 3 and 4, typical of mass fractals (inset table in Figure 7). The hydrogels showed lower slopes, in agreement with a conformational change due to the swelling and expansion of the network induced by the hydration of the polypeptide chains [35,36]. The hydrogels equilibrated at pH 4 and 5 showed power-law behaviour up to 0.038 Å^{-1} and slopes between 2 and 2.6. On the other hand, the hydrogels equilibrated at pH 6, 7 and 8 presented this behaviour up to 0.023 Å^{-1} with slopes values near 1. As aforementioned, the lower slope than at low pHs is indicative of expanded networks, and values near 1 account for rod-like structures [37]. Beaucage proposed a unified equation for the analysing of disordered materials with more than one structural levels [36]:

$$I(q) \approx G^{\left(\frac{-q^2R_g^2}{3}\right)} + B^{\left(\frac{-q^2R_{sub}^2}{3}\right)}\left(\frac{1}{q^*}\right)^{p} + G^{\left(\frac{-q^2R_s^2}{3}\right)} + B_s\left(\frac{1}{q_s^*}\right)^{P_s} \qquad (1)$$

where G and G_s are the Guinier prefactors for the larger and smaller structures respectively,

R_g is the radius of gyration, R_s is the smallest R_g observed at high q, whereas R_{sub} is at the high q limit, B and B_s are prefactors specific to the Power-law scattering, which are specified as the decay exponent P and P_s respectively, $q^* = q/[\mathrm{erf}(q\ k\ R_g/6^{1/2})]^3$ and $q_s^* = q/[\mathrm{erf}(q\ k_s\ R_s/6^{1/2})]^3$.

The calculated R_g values for the rod-like structure can be seen as the inset table in Figure 7. All samples at the expanded pHs presented R_g values in a range of 125 to 145 nm. Kox R_g values were lower than Ker ones but with varying values between batches (data not shown). Thus, these values do no imply a clear trend. This would imply that the introduction of $-SO_3^-$ groups did not significantly alter the main conformation adopted by the polypeptide chain. Nevertheless, all α values at every condition were lower for Kox profiles than for the Ker ones. Thus, it can be proposed that the introduction of sulfonic groups is not as influential enough to change the protein nanometric conformation but the hydration or repulsion generated for these groups leads to a greater expansion among the protein chains or rod-like structures. In addition, this greater expansion and swelling of the hydrated Kox chains would be possible due to the higher mobility of the network gained with the oxidation, as observed by ^{1}H HRMAS NMR. In this regard, the SAXS profiles of the dry materials can help to understand the origin of this observed trend. The dry Ker profile showed a correlation peak that represents a distance of 47 Å according to Bragg's law ($d = 2\pi/q$), assigned to an ordered structure that appeared in Ker after the synthesis since it is not present in pristine horn keratin [12]. During the synthesis, the amount of α-helix domains from pristine keratin unfold to form disordered and more mobile domains. This greater mobility allowed the remaining β-sheets domains to pack orderly, giving rise to the peak observed in dry Ker profile. This peak was not present for the dry Kox profile. Therefore, it can be expected that some of the remaining β-sheets domains would become disordered after the oxidation, allowing the hydrogels to achieve higher expansion and swelling that the Ker hydrogels.

In order to understand the effect of the selective ion responsiveness, SD 12 compares the SAXS profiles of Ker and Kox hydrogels equilibrated at pH 8, pH 4 and equilibrated at pH 8 in the presence of 100 mM Ca^{2+}. Both Ker and Kox profiles equilibrated at pH 8 in the presence of Ca^{2+} show a power-law behaviour up to 0.029 $Å^{-1}$ with a slope similar to the ones observed for the hydrogels equilibrated at pH 4. Although lower slope would be expected according to the media pH, the interaction of Ca^{2+} ions is strong enough to disorder the polypeptide chain and induce their contraction leading to lower swellings.

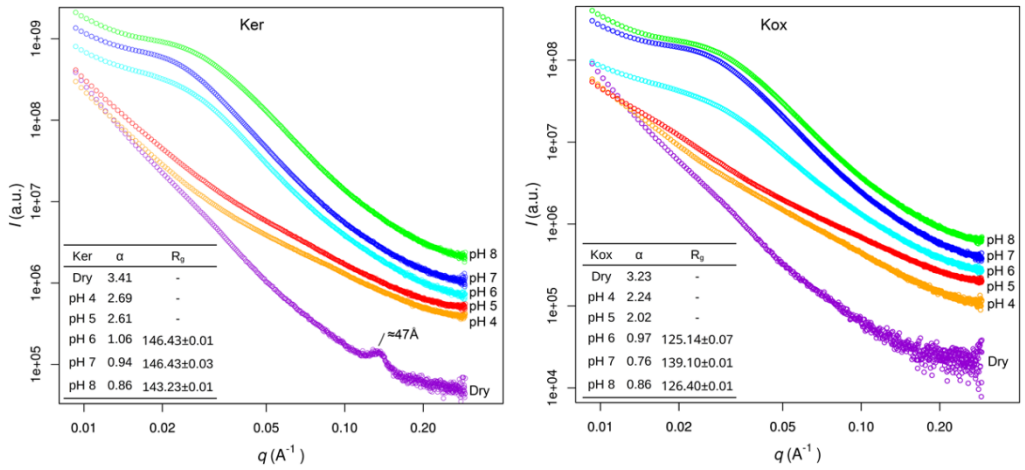

Figure 7. SAXS profiles of the Ker and Kox 20% dry materials and hydrogels equilibrated at different pHs.

Conclusions

In this work the obtaining of a keratose hydrogel was achieved while maintaining the reversible stimuli responsive behaviour from the original keratin hydrogel. Hydrogen peroxide and temperature were relevant parameters of the oxidation of -SH and -S-S- groups to $-SO_3^-$ while preserving the 3D structure of the hydrogels and the primary sequence of the protein. The comparison of the stimuli-responsiveness of keratin and keratose hydrogel showed that the latter can achieve higher swelling than the former. This property was ascribed to a loss in keratin secondary structure, probably due to a decrease in β-sheets domains, together with the gaining of sulfonic acid groups that allows higher mobility, and expansion and water uptake of the polypeptide chain.

The stimuli-responsive behaviour of these hydrogels is not electrostatic repulsion/attraction driven but is originated in the polypeptide conformational change, and maintained after the oxidation into keratose. The hydrogels showed reversible stimuli-responsive behaviour towards media pH and specific ions presence, in particular to Ca^{2+} at the expanded form and to Cu^{2+} at the contracted forms, respectively. This pH and cations triggered response of Ker and Kox hydrogels show these materials promising candidates for their application as sensors or drug delivery systems.

Acknowledgements

G.G. is grateful for his undergraduate fellowship granted by Universidad de Buenos Aires (UBA). The authors are grateful to the Brazilian Synchrotron Light Laboratory (LNLS) for SAXS facilities and would like to acknowledge INTI Mecánica and M. Pianetti for their assistance in SEM analysis. This work was supported with grants from Universidad de

Buenos Aires (UBACYT 20020170100125BA) and Agencia Nacional de Promoción Científica y Tecnológica (PICT 2015-0714, PICT 2016-1997). The authors acknowledge the XPS and thermogravimetric measurements performed under the frame of "Ministerio de Economía y Competitividad" MAT2016-76739-R (AEI/FEDER, EU). The authors would like to thank I. Pickering for language corrections.

Research data for this article

Data not available / Data will be made available on request

References

[1] Yang X., Zhang H., Yuan X., Cui S., : Wool keratin: A novel building block for layer-by-layer self-assembly. Journal of Colloid and Interface Science. **336**, 756–760 (2009). DOI:10.1016/j.jcis.2009.04.050.

[2] Ham T.R., Lee R.T., Han S., Haque S., Vodovotz Y., Gu J., Burnett L.R., Tomblyn S., Saul J.M., : Tunable Keratin Hydrogels for Controlled Erosion and Growth Factor Delivery. Biomacromolecules. **17**, 225–236 (2016). DOI:10.1021/acs.biomac.5b01328.

[3] Fernández-d'Arlas B., : Improved aqueous solubility and stability of wool and feather proteins by reactive-extraction with H2O2 as bisulfide (-S-S-) splitting agent. European Polymer Journal. **103**, 187–197 (2018). DOI:10.1016/j.eurpolymj.2018.04.010.

[4] Tonin C., Zoccola M., Aluigi A., Varesano A., Montarsolo A., Vineis C., Zimbardi F., : Study on the Conversion of Wool Keratin by Steam Explosion. Biomacromolecules. **7**, 3499–3504 (2006). DOI:10.1021/bm060597w.

[5] Xu W., Ke G., Wu J., Wang X., : Modification of wool fiber using steam explosion. European Polymer Journal. **42**, 2168–2173 (2006). DOI:10.1016/j.eurpolymj.2006.03.026.

[6] de Guzman R.C., Merrill M.R., Richter J.R., Hamzi R.I., Greengauz-Roberts O.K., Van Dyke M.E., : Mechanical and biological properties of keratose biomaterials. Biomaterials. **32**, 8205–8217 (2011). DOI:10.1016/j.biomaterials.2011.07.054.

[7] Yang G., Yao Y., Wang X., : Comparative study of kerateine and keratose based composite nanofibers for biomedical applications. Materials Science and Engineering: C. **83**, 1–8 (2018). DOI:10.1016/j.msec.2017.07.057.

[8] Barati D., Kader S., Pajoum Shariati S.R., Moeinzadeh S., Sawyer R.H., Jabbari E., : Synthesis and Characterization of Photo-Cross-Linkable Keratin Hydrogels for Stem Cell Encapsulation. Biomacromolecules. **18**, 398–412 (2017). DOI:10.1021/acs.biomac.6b01493.

[9] Ferroni C., Sotgiu G., Sagnella A., Varchi G., Guerrini A., Giuri D., Polo E., Orlandi V.T., Marras E., Gariboldi M., Monti E., Aluigi A., : Wool Keratin 3D Scaffolds with Light-Triggered Antimicrobial Activity. Biomacromolecules. **17**, 2882–2890 (2016). DOI:10.1021/acs.biomac.6b00697.

[10] Guo J., Pan S., Yin X., He Y.-F., Li T., Wang R.-M., : pH-sensitive keratin-based polymer hydrogel and its controllable drug-release behavior. Journal of Applied Polymer Science. n/a-n/a (2014). DOI:10.1002/app.41572.

[11] Sun K., Guo J., He Y., Song P., Xiong Y., Wang R.-M., : Fabrication of dual-sensitive keratin-based polymer hydrogels and their controllable release behaviors. Journal of Biomaterials Science, Polymer Edition. **27**, 1926–1940 (2016). DOI:10.1080/09205063.2016.1239955.
[12] Peralta Ramos M.L., González J.A., Fabian L., Pérez C.J., Villanueva M.E., Copello G.J., : Sustainable and smart keratin hydrogel with pH-sensitive swelling and enhanced mechanical properties. Materials Science and Engineering: C. **78**, 619–626 (2017). DOI:10.1016/j.msec.2017.04.120.
[13] Peralta Ramos M.L., Galaburri G., González J.A., Pérez C.J., Villanueva M.E., Copello G.J., : Influence of GO reinforcement on keratin based smart hydrogel and its application for emerging pollutants removal. Journal of Environmental Chemical Engineering. **6**, 7021–7028 (2018). DOI:10.1016/j.jece.2018.11.011.
[14] Villanueva M.E., Cuestas M.L., Pérez C.J., Campo Dall′ Orto V., Copello G.J., : Smart release of antimicrobial ZnO nanoplates from a pH-responsive keratin hydrogel. Journal of Colloid and Interface Science. **536**, 372–380 (2019). DOI:10.1016/j.jcis.2018.10.067.
[15] Shang J., Le X., Zhang J., Chen T., Theato P., : Trends in polymeric shape memory hydrogels and hydrogel actuators. Polymer Chemistry. **10**, 1036–1055 (2019). DOI:10.1039/C8PY01286E.
[16] Liang R., Wang L., Yu H., Khan A., Ul Amin B., Khan R.U., : Molecular design, synthesis and biomedical applications of stimuli-responsive shape memory hydrogels. European Polymer Journal. **114**, 380–396 (2019). DOI:10.1016/j.eurpolymj.2019.03.004.
[17] Wojdyr M., : Fityk : a general-purpose peak fitting program. Journal of Applied Crystallography. **43**, 1126–1128 (2010). DOI:10.1107/S0021889810030499.
[18] Paquin R., Colomban P., : Nanomechanics of single keratin fibres: A Raman study of the α-helix →β-sheet transition and the effect of water. Journal of Raman Spectroscopy. **38**, 504–514 (2007). DOI:10.1002/jrs.1672.
[19] Nielsen S.S., Toft K.N., Snakenborg D., Jeppesen M.G., Jacobsen J.K., Vestergaard B., Kutter J.P., Arleth L., : BioXTAS RAW, a software program for high-throughput automated small-angle X-ray scattering data reduction and preliminary analysis. Journal of Applied Crystallography. **42**, 959–964 (2009). DOI:10.1107/S0021889809023863.
[20] Breßler I., Kohlbrecher J., Thünemann A.F., : SASfit: a tool for small-angle scattering data analysis using a library of analytical expressions. Journal of Applied Crystallography. **48**, 1587–1598 (2015). DOI:10.1107/S1600576715016544.
[21] Lopez-Ramon M.V., Stoeckli F., Moreno-Castilla C., Carrasco-Marin F., : On the characterization of acidic and basic surface sites on carbons by various techniques. Carbon. **37**, 1215–1221 (1999). DOI:10.1016/S0008-6223(98)00317-0.
[22] R Development Core Team, R: A Language and Environment for Statistical Computing, R Foundation for Statistical Computing, Vienna, Austria, 2009. http://www.R-project.org.
[23] Edwards H.G.M., Hunt D.E., Sibley M.G., : FT-Raman spectroscopic study of keratotic materials: horn, hoof and tortoiseshell. Spectrochimica Acta Part A: Molecular and Biomolecular Spectroscopy. **54**, 745–757 (1998). DOI:10.1016/S1386-1425(98)00013-4.
[24] Richardson M.J., Johnston J.H., : Sorption and binding of nanocrystalline gold by Merino wool fibres—An XPS study. Journal of Colloid and Interface Science.

310, 425–430 (2007). DOI:10.1016/j.jcis.2007.01.075.
[25] Florence T.M., : Degradation of protein disulphide bonds in dilute alkali. The Biochemical Journal. **189**, 507–520 (1980).
[26] Milczarek P., Zielinski M., Garcia M.L., : The mechanism and stability of thermal transitions in hair keratin. Colloid and Polymer Science. **270**, 1106–1115 (1992). DOI:10.1007/BF00652875.
[27] Zhang Q., Shan G., Cao P., He J., Lin Z., Huang Y., Ao N., : Mechanical and biological properties of oxidized horn keratin. Materials Science and Engineering: C. **47**, 123–134 (2015). DOI:10.1016/j.msec.2014.11.051.
[28] Brebu M., Spiridon I., : Thermal degradation of keratin waste. Journal of Analytical and Applied Pyrolysis. **91**, 288–295 (2011). DOI:10.1016/j.jaap.2011.03.003.
[29] Li B., Yao J., Niu J., Liu J., Wang L., Feng M., Sun Y., : Effects of Graphene Oxide on the Structure and Properties of Regenerated Wool Keratin Films. Polymers. **10**, 1318 (2018). DOI:10.3390/polym10121318.
[30] Kayser J., Grabmayr H., Harasim M., Herrmann H., Bausch A.R., : Assembly kinetics determine the structure of keratin networks. Soft Matter. **8**, 8873 (2012). DOI:10.1039/c2sm26032h.
[31] Martin I., Moch M., Neckernuss T., Paschke S., Herrmann H., Marti O., : Both monovalent cations and plectin are potent modulators of mechanical properties of keratin K8/K18 networks. Soft Matter. **12**, 6964–6974 (2016). DOI:10.1039/C6SM00977H.
[32] Shestakova P., Willem R., Vassileva E., : Elucidation of the Chemical and Morphological Structure of Double-Network (DN) Hydrogels by High-Resolution Magic Angle Spinning (HRMAS) NMR Spectroscopy. Chemistry - A European Journal. **17**, 14867–14877 (2011). DOI:10.1002/chem.201101334.
[33] Asakura T., Endo M., Hirayama M., Arai H., Aoki A., Tasei Y., : Glycerin-Induced Conformational Changes in Bombyx mori Silk Fibroin Film Monitored by 13C CP/MAS NMR and 1H DQMAS NMR. International Journal of Molecular Sciences. **17**, 1517 (2016). DOI:10.3390/ijms17091517.
[34] Lázaro-Martínez J.M., Rodríguez-Castellón E., Vega D., Monti G.A., Chattah A.K., : Solid-state Studies of the Crystalline/Amorphous Character in Linear *Poly* (ethylenimine hydrochloride) (PEI·HCl) Polymers and Their Copper Complexes. Macromolecules. **48**, 1115–1125 (2015). DOI:10.1021/ma5023082.
[35] Brinker C.J., Keefer K.D., Schaefer D.W., Assink R.A., Kay B.D., Ashley C.S., : Sol-gel transition in simple silicates II. Glasses and Glass Ceramics from Gels. **63**, 45–59 (1984). DOI:10.1016/0022-3093(84)90385-5.
[36] Beaucage G., : Small-Angle Scattering from Polymeric Mass Fractals of Arbitrary Mass-Fractal Dimension. Journal of Applied Crystallography. **29**, 134–146 (1996). DOI:10.1107/S0021889895011605.
[37] Schmitt C., Moitzi C., Bovay C., Rouvet M., Bovetto L., Donato L., Leser M.E., Schurtenberger P., Stradner A., : Internal structure and colloidal behaviour of covalent whey protein microgels obtained by heat treatment. Soft Matter. **6**, 4876 (2010). DOI:10.1039/c0sm00220h.

Graphical abstract

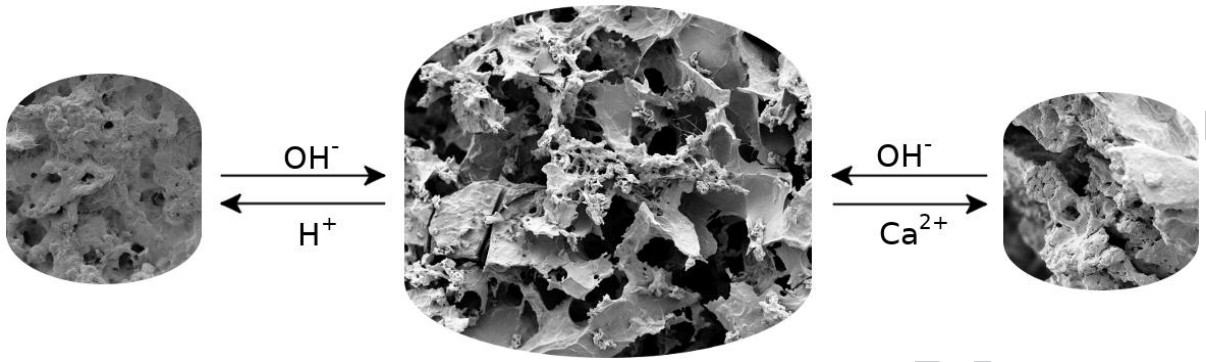

Highlights

>Dual-responsive keratin hydrogels were oxidized to keratose hydrogels

>Keratose hydrogels presented steeper stimuli responsiveness

>H_2O_2 oxidation of -SS- at β-sheets domains allowed higher swellings in keratose >A non-described selective ion-responsiveness is presented

>Ca(II) at high pH and Cu(II) at low pH induce shrinking and swelling respectively